BeppoSAX observations of Mkn 3:
Piercing through the torus of a Seyfert 2 galaxy

M. Cappi[1], **L. Bassani**[1], **A. Comastri**[2], **M. Guainazzi**[3], **T. Maccacaro**[4], **G. Malaguti**[1], **G. Matt**[5], **G.G.C. Palumbo**[6,1], **P. Blanco**[7], **M. Dadina**[8], **D. Dal Fiume**[1], **G. Di Cocco**[1], **A.C. Fabian**[9], **F. Frontera**[1], **R. Maiolino**[10], **L. Piro**[11], **M. Trifoglio**[1], and **N. Zhang**[12]

[1] Istituto TeSRE-CNR, Via Gobetti 101, I-40129 Bologna, Italy
[2] Osservatorio Astronomico di Bologna, Via Ranzani 1, I-40127 Bologna, Italy
[3] Astrophysics Division, SCD -ESA, ESTEC, Postbus 299, 2200 AG Noordwijk, The Netherlands
[4] Osservatorio Astronomico di Brera, Via Brera 28, I-20121 Milano, Italy
[5] Dipartimento di Fisica, Universita' di RomaIII, Via della Vasca Navale 84, I-00146 Roma, Italy
[6] Dipartimento di Astronomia, Universita' di Bologna, Via Ranzani 1, I-40127 Bologna, Italy
[7] UCSD, San Diego-Ca, USA
[8] BeppoSAX S.D.C., ASI, Via Corcolle 19, I-00131 Rome, Italy
[9] Institute of Astronomy, Cambridge University, Madingley Road, Cambridge CB3 0HA, UK
[10] Osservatorio Astrofisico di Arcetri, Via L.E. Fermi 5, I-5015 Firenze, Italy
[11] Istituto di Astrofisica Spaziale, Via Del Fosso del Cavaliere, I-001333 Roma, Italy
[12] University Space Research Association, Huntsville-Al, USA

Abstract. A new $BeppoSAX$ broad-band (0.6–150 keV) spectrum of the Seyfert 2 galaxy Mkn 3 is presented. The spectrum provides a direct measurement of a large, neutral column of gas with $N_H \sim 10^{24}$ cm^{-2} in the source direction. The source, as bright as 3C 273 above 10 keV, has a steep ($\Gamma \sim 1.8$) spectrum without any evidence of a high-energy cutoff up to at least 150 keV. At lower energies, the data are best modeled with the addition of an unabsorbed reflection component. Combining these data with previous $Ginga$ and $ASCA$ observations, the Fe K$_\alpha$ and reflection continuum indicate that the reprocessed emission is responding slower than the intrinsic continuum variations suggesting a size of the reprocessor $\gtrsim 2$ pc. Identifying such a reprocessor with a (close to edge-on) obscuring torus, the overall result fits well into unified models since, presumably, one can interpret the strong absorption as due to transmission through the rim of the torus and the unabsorbed (directly viewed) reflection component as due to reprocessing from the torus inner surface.

Key words: galaxies: individual: Mkn 3 – galaxies: Seyfert – X-rays: galaxies

1. Introduction

It has long been recognized that the hard X-ray spectra of Seyfert galaxies (at E $\gtrsim$ 20 keV, photo-electric absorption becomes inefficient) are a powerful tool for extracting information on the intrinsic source emission properties (i.e. luminosity and spectral shape). Such measurements are fundamental for the understanding of the emission mechanisms operating in these objects and, since they allow a direct comparison between different classes of AGNs (e.g. Seyfert 1 versus Seyfert 2 galaxies), for testing unified models (Antonucci 1993). At lower energies ($\sim$ 0.1–20 keV), one can obtain information on column densities, ionization and abundances of the surrounding matter. This issue is important in testing the geometry and in particular the existence of molecular tori with $N_H \gtrsim 10^{24}$ cm^{-2} around Seyfert galaxies whose presence is essential for AGN unified models and synthesis models of the X-ray background.

In the few $OSSE$ data available for Seyfert galaxies, the steep high-energy spectra, the evidence of a high-energy cutoff (e.g. Maisack et al. 1993, Zdziarski et al. 1995, Grandi et al. 1998), and the absence of an annihilation line favour thermal Comptonization models (Haardt 1997) in contrast with the predictions from non-thermal pair models (see Svensson 1994 for a review). More precise measurements by $BeppoSAX$ have confirmed the presence of high-energy cutoffs in some Seyfert 1 galaxies (Piro et al. 1999) though only lower-limits have been found in others (Perola et al. 1999). To date, however, precise measurements are still lacking for Seyfert 2 galaxies with only a few attempted (Zdziarski et al. 1995, Bassani et al. 1995, Weaver et al. 1998), and, as such, fundamental to be performed.

Mkn 3 (z=0.0135) is one of the small sample of Seyfert 2 galaxies which show broad emission lines in polarized light suggesting the presence of a "hidden Seyfert 1 nucleus" (e.g., Miller & Goodrich 1990 and Tran 1995). Other evidence in favor of heavy obscuration are: the discovery of a biconical extended narrow line region (Pogge & De Robertis 1993), the low flux of

ionizing photons inferred from the directly observed UV continuum compared to the ionizing photons required to produce the observed Hβ emission (Haniff et al. 1988, Wilson et al. 1988), the low $L_X/L_{[OIII]}$ ratio (0.14; Bassani et al. 1998) and the observation of heavy X-ray obscuration. Indeed, *Ginga* data have shown that the spectrum of Mkn 3 is flat ($\Gamma \sim 1.3$), absorbed by a column density of $N_H \sim 6 \times 10^{23}$ cm^{-2} and has a strong iron line with equivalent width (EW) ~ 500 eV (Awaki et al. 1991). Measurements at low X-ray energies revealed the presence of a soft excess and also indicated the presence of prominent soft X-ray emission lines (Kruper et al. 1990, Turner et al. 1993, Iwasawa et al. 1994 (I94 hereinafter)). The *ASCA* observation revealed that the Fe K_α line emission decreased by a factor of 3 in response to a flux decline by a factor of 6 (I94). *ASCA* also resolved the iron line in a 6.4 keV component of EW $\sim$ 900 eV and a 6.7 keV one of EW $\sim$ 190 eV (I94). The analysis of the same data set alone, or in combination with measurements from other instruments, indicated the difficulty encountered in interpreting unequivocally the 2–10 keV spectrum (Turner et al. 1997a,b and Griffiths et al. 1998, G98 hereinafter). It also highlighted the need for a broad-band coverage to better interpret the observed emission. At high energies, Mkn 3 was detected by *OSSE* for the first time in March 1994 at a flux level of $\sim 2.8 \times 10^{-11}$ erg cm^{-2} s^{-1} in the 50–150 keV energy band (Johnson, private communication).

Here we present the observation of Mkn 3 by *BeppoSAX*. The results obtained highlight the potentialities of using *BeppoSAX* in broad-band X-ray spectroscopy studies of active galactic nuclei, in particular in the case of highly absorbed sources like Seyfert 2 galaxies. Throughout the analysis, we use $H_o = 50$ km s^{-1} Mpc^{-1} and q_o=0.

2. Observations and data reduction

The *BeppoSAX* narrow field instruments consist of one low-energy concentration spectrometer (LECS, Parmar et al. 1997), three medium energy concentrator spectrometers (MECS, Boella et al. 1997), a high pressure gas scintillation proportional counter (HPGSPC, Manzo et al. 1997), and a phoswich detector system (PDS, Frontera et al. 1997) covering the 0.1–10 keV, 1.3–10 keV, 4–120 keV and 13–300 keV energy ranges, respectively. HPGSPC data will not be considered in the present paper since the source is too faint for a correct background subtraction and we restricted the spectral analysis to the 0.1–4.5 keV and 1.5–10 keV energy bands for the LECS and MECS, respectively, where the latest released (September 1997) response matrices are best calibrated. The LECS data were ignored below 0.6 keV, i.e. below the lowest energy at which Mkn 3 is detected at the 3 σ level.

Mkn 3 was observed for about two days using all the above instruments during the period April 16–18, 1997. The total effective exposure was 39433 s in the LECS, 113690 s in the MECS and 51386 s in the PDS. Light-curves and spectra were extracted (using the ftools v4.0 software package) from within a region of $\sim 4'$ radius centered on the source for both LECS and MECS instruments. Standard blank-sky files provided by

the *BeppoSAX* Science Data center (SDC) were used for the background subtraction. Similar results were obtained using the background spectra extracted directly from the instruments fields of view (FOVs). The 3 MECS instruments gave consistent timing and spectral results if taken individually and were, thus, added together. In the LECS and MECS FOVs, we also detected emission in the direction of the BL Lac object MS 0607.9+7108 about 6–7$'$ NW of Mkn 3, that certainly lies also in the PDS FOV (which has a triangular response with FWHM of $\sim 1.3°$, Frontera et al. 1997). Although the statistics are too poor for a detailed spectral analysis of this source, we can, however, exclude the possibility of contamination for the present analysis because a) it is weak (about 1/100 the 2–10 keV flux of Mkn 3) and b) its spectrum is steep as indicated by the fact that its detection is clear in the LECS FOV but marginal in the MECS FOV. Similar considerations were also reported by I94 and G98. Searches in high-energy catalogues reveal no other likely contaminating source within the 1.3° FOV of the PDS.

In total, the source count-rates were $(6.8\pm0.5) \times 10^{-3}$ cts s^{-1} in the LECS and $(6.95\pm0.08) \times 10^{-2}$ cts s^{-1} in the MECS, the background contributing $\sim 20\%$ at 6 keV and $\sim$ 7% at 8 keV, respectively. No significant variability was found within the statistical fluctuations of $\sim 15\%$ (MECS data), thus all data were accumulated over the whole observation. The PDS data reduction was performed using both XAS (v.2.0, Chiappetti & Dal Fiume 1997) and SAXDAS (v.1.3.0.) software packages and yielded consistent results. In the following, we'll refer to the results obtained with the XAS package. The source count-rate in the PDS was 1.16 ± 0.02 cts s^{-1} which corresponds to a total of $\sim 50\,\sigma$ detection in the 13–150 keV energy range and $\sim 7\,\sigma$ between 100–150 keV. No significant variability was found but we cannot exclude variations up to a factor ~ 2 (corresponding to the statistical fluctuations) within the entire observation.

For the spectral analysis, the LECS and MECS data were rebinned such as to sample the instrument resolution with a number of 1 and 5 channels per energy bin, respectively (about $\gtrsim 20$ and 50 cts bin^{-1}). The PDS data were grouped logarithmically between 13–200 keV, with a S/N ratio $\gtrsim 3$ per bin. The spectral analysis was performed using version 10.00 of the XSPEC program (Arnaud 1996).

3. Spectral analysis

3.1. The PDS high-energy spectrum

A simple power-law fit (with $\Gamma \simeq 1.61 \pm 0.05$; where $N_E \propto E^{-\Gamma}$) over the entire energy range (~ 13–200 keV) of the PDS data, is clearly unacceptable because below ~ 20 keV the data are systematically lower than the model, yielding a poor fit with a $\chi^2 = 47$ for 28 d.o.f. (χ^2_{red}=1.68, rejected at 99.8% level in terms of χ^2 statistics). With absorption added to the model, the fit becomes acceptable with: $\Gamma \simeq 1.79 \pm 0.12$, $N_H \simeq (1.54 \pm 0.70) \times 10^{24}$ cm^{-2} and $\chi^2 = 32.28$ for 27 d.o.f. (χ^2_{red}=1.19). Here and below, errors are at 90% confidence for one interesting parameter unless otherwise stated. Best-fit spectrum, residuals and χ^2 contour plots in the parameter space N_H–Γ are shown in Fig. 1. If a 10% systematic error is added to the data below 20 keV to
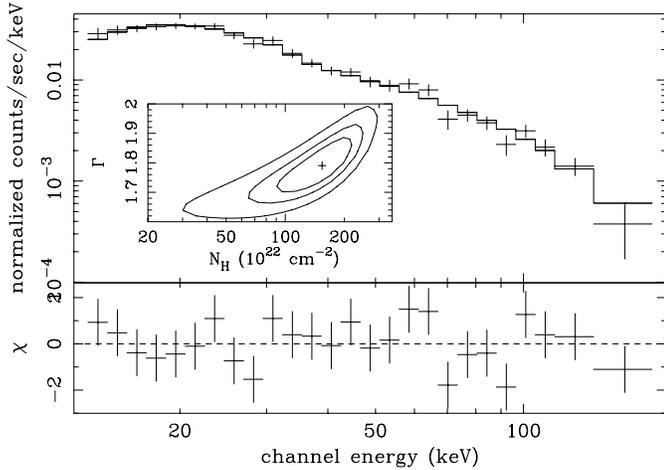
Fig. 1. Background subtracted PDS (13–150 keV) spectrum and residuals. Note that each data point has a S/N $\gtrsim$ 3. Inserted figures shows the χ^2 contour plots in the N_H-Γ parameter space with solid line contours indicating the 68%, 90% and 99% confidence limits.

Fig. 2. Residuals (in units of standard deviation) of the LECS, MECS and PDS broad-band spectrum for a model consisting of a single power-law with $\Gamma \sim 0.45$. This figure illustrates the soft excess below $\sim$ 3 keV, the strong Fe K$_\alpha$ line at $\sim$ 6.4 keV and the sharp rise and fall of the spectrum at $E \gtrsim$ 10 keV.

account for residual calibration uncertainties at those energies (Dal Fiume 1998, private communication), we find somewhat larger ($\sim$ 20%) errors on Γ and N_H but the derived best-fit values remain unchanged. The observed (absorbed) 13–150 keV flux is about 1.47×10^{-10} ergs cm^{-2} s^{-1}, which makes Mkn 3 one of the brightest known AGNs in the hard X-ray energy range, as bright as 3C 273 (Haardt et al. 1998) and the buried Seyfert 2 galaxy NGC 4945 (Done et al. 1996). Comparison with the *OSSE* observations (Sect. 1) indicates that the source varied by at least a factor 3 in the 50–150 keV energy range.

3.2. The 0.6–150 keV broad-band spectrum: baseline model

Given the source spectral complexity (in particular below 10 keV), we addressed separately, in Appendix A, the study of the data below 10 keV *alone*. This allows us to compare *BeppoSAX* results to the ones previously reported in the literature, and to illustrate the ambiguities encountered in interpreting the spectrum of Mkn 3 over such a limited energy range. In the following, the results obtained for the overall broad-band spectrum are presented.

The data sets from LECS (0.6–4.5 keV), MECS (2.5–10 keV) and PDS (13–150 keV) detectors were fitted simultaneously. To allow for differences in the absolute flux calibration of the individual detectors, the normalization of different instruments was allowed to vary within 20% of the fiducial values of $A_{LECS}/A_{MECS} = 0.65$ and $A_{PDS}/A_{MECS} = 0.85$ (e.g., Haardt et al. 1998). Unless differently stated, the ratios obtained from the fits were all within $\sim$ 5% of these fiducial values. A column density $N_{HGal} = 8.46 \times 10^{20}$ cm^{-2} due to absorption by the Galaxy (Dickey & Lockman 1990), was included in all models used in the following.

In Fig. 2, we show the residuals obtained between 0.6 and 150 keV for a fit with a power-law model plus Galactic absorption. The fit (where $\Gamma \simeq 0.4$) clearly illustrates the complex
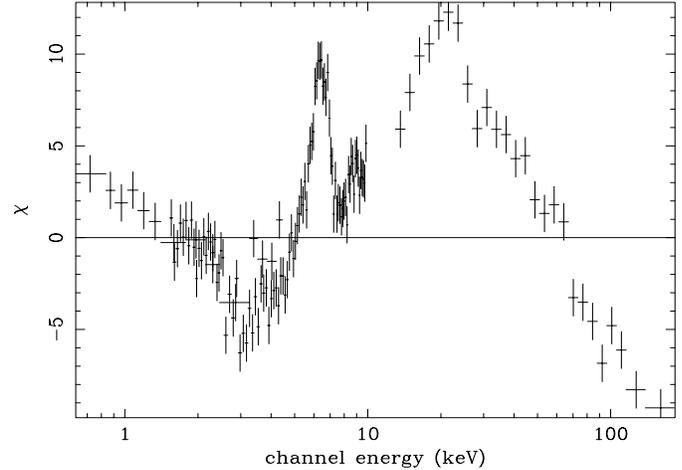
spectral structure below 10 keV (see also Appendix A) and the strong and sharp "rise and fall" of the spectrum above 10 keV.

Because of the presence of the very strong Fe K$_\alpha$ line, we first attempted to fit the overall broad-band spectrum with a pure reflection model[1] plus a steep soft power-law continuum that accounts for the low-energy emission below $\sim$ 3 keV. Such a model is however ruled out ($\chi^2_{red} \simeq 2$) since it falls short of the data between 8–20 keV for any value of photon index, cutoff, inclination and ionization state of the reflecting material. This clearly indicates that the sharp rise and fall observed above $\sim$ 10 keV cannot be explained *only* by the presence of an unabsorbed reflection component but requires, instead, the presence of a direct, strongly absorbed power-law component as modeled in Sect. 3.1.

In Appendix A, we show that a model consisting of a soft power-law continuum, an iron line plus a strongly absorbed hard power-law continuum (as initially proposed by I94) gives an acceptable description of the data below 10 keV. In the broad-band spectrum, however, we find that such model is ruled out ($\chi^2_{red} \simeq 1.4$, Table 1) since it falls short of the data by a factor of about 2 in the PDS energy range. The continuum below the line (from about 3 to 8 keV) is extremely flat, thus a simple transmission model from cold matter (even with $N_H \simeq 7$–10×10^{23} cm^{-2}) cannot *simultaneously* fit the low and high energy bands. Similar results are obtained if one considers an ionized absorber instead of a neutral one.

A better solution is found, instead, with a basic description (called "baseline" model in the following) as first proposed by

---

[1] The reflection model used is the *pexrav* model in XSPEC which is an exponentially cutoff power-law spectrum reflected from a plane of neutral, optically thick, material (Magdziarz & Zdziarski 1995). Inclination and abundances were fixed to the standard values, $\sim$ 60° and 1, respectively. The cutoff energy of the primary power-law spectrum (E_c) were frozen at 1000 keV, unless otherwise stated.
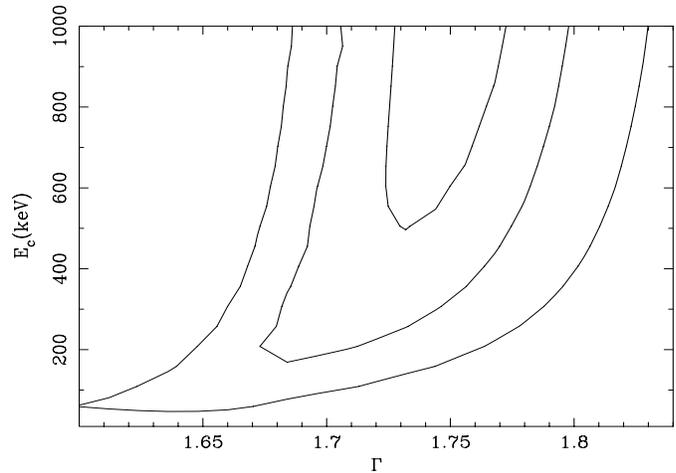
Table 1. Fits of the broad band spectrum

Continuum Model[a]	Γ_s	A_s/A_h $\times 10^{-2}$	N_H^b	Γ_h	R	$E_{K\alpha}^c$	$\sigma_{K\alpha}^d$	$A_{K\alpha}^e$	χ_{red}^2/χ^2/d.o.f.
pl_s+abs.pl_h	$1.02^{+0.18}_{-0.14}$	1.1	109^{+16}_{-10}	$1.75^{+0.08}_{-0.11}$	-	$6.49^{+0.07}_{-0.07}$	$0.23^{+0.14}_{-0.11}$	$4.9^{+1.7}_{-1.3}$	1.41/186/132
baseline: pl_s+refl.+abs.pl_h	$2.64^{+0.41}_{-0.79}$	2.3	127^{+24}_{-22}	$1.79^{+0.06}_{-0.12}$	$0.95^{+0.12}_{-0.15}$	$6.47^{+0.09}_{-0.12}$	$0.22^{+0.16}_{-0.15}$	$4.6^{+1.7}_{-1.3}$	0.93/121/131

[a] See text for descriptions.
[b] in units of 10^{22} cm^{-2}.
[c] Line energy in the source rest-frame, in units of keV.
[d] Line width, in units of keV.
[e] *Observed* line intensity in units of 10^{-5} photons cm^{-2} s^{-1}.

Note: Intervals are at 90% confidence for 2 interesting parameters.
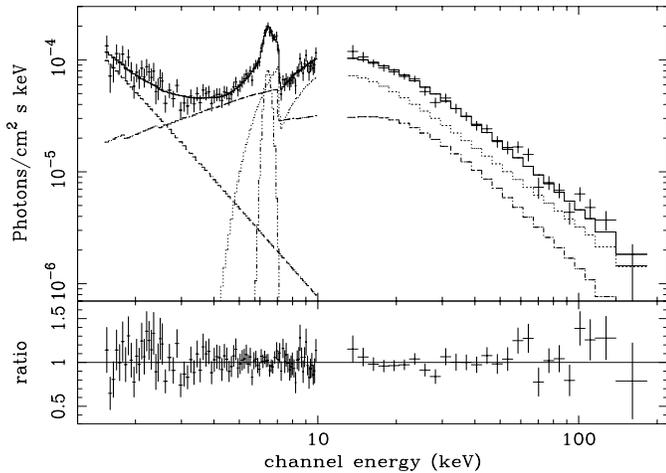
Fig. 3. Unfolded broad-band spectrum and baseline model obtained by fitting the LECS, MECS and PDS data. For clarity, only the MECS and PDS data are shown here.

Fig. 4. χ^2 contour plots in the Γ-E_c parameter space. Solid line contours represent the 68%, 90% and 99% confidence limits.

Turner et al. (1997b) that includes a soft power-law component, a strongly absorbed power-law component and an iron line plus an *unabsorbed* reflection[1] component. Photon index and normalization of the primary power-law were assumed to be those of the hard, absorbed, power-law component. In this simplest form, this model adds only 1 free parameter (R), namely the relative amount of reflection compared to the directly-viewed primary power-law. The case R=1 corresponds to a 2π coverage as viewed from the X-ray source. The best-fit parameters obtained from this baseline model are given in line 2 of Table 1. The unfolded spectrum and data-model ratios are given in Fig. 3.

The cutoff energy (E_c) of the primary power-law continuum was then allowed to vary to search for a high-energy cutoff in the data. The fit gives a lower limit of $E_c \gtrsim 200$ keV at 90% confidence (see Fig. 4). However, given the 10% systematic uncertainty between the MECS and PDS normalizations (Cusumano et al. 1998), we estimated an additional ~ 50 keV systematic error on this limit. It is stressed that it is difficult to obtain a very stringent limit on E_c in this source because its intrinsic spectrum only emerges at E$\gtrsim$20 keV, where with the present data it is difficult to statistically sort out the parameters R, N_H, Γ, and E_c. However, looking at Fig. 3, we underline the

clear absence of any cutoff at high energies up to about 150 keV. In conclusion, if a cutoff does exist, it occurs at energies above ~ 150 keV.

The adopted baseline model (admittedly rather complex) is, however, too simple to describe correctly the overall complexity of the spectrum of Mkn 3. In the following section, we discuss point by point the several "deviations" from the baseline model that are required by the data. For completeness, more complex models, alternative to the proposed baseline model, are presented in Appendix B. Statistically, they represent viable alternative descriptions of the broad-band spectra. However, they were discarded on the basis of physical arguments and lack of simplicity (Occam's razor).

3.3. "Optimizations" of the baseline model

First of all, in constructing the baseline model the absorption model used only considers photo-electric absorption and neglects Compton scattering which, however, becomes relevant for $N_H \gtrsim 10^{24}$ cm^{-2} (Ghisellini et al. 1994, Yaqoob 1997). To take this effect into account, we used *plcabs* in XSPEC which describes the X-ray transmission through a uniform, spherical distribution of matter, correctly taking into account Compton
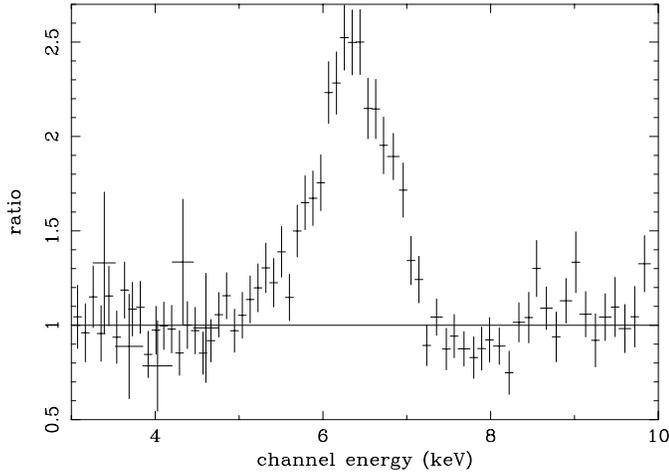
Fig. 5. Iron line feature obtained from fitting the LECS + MECS spectrum between 3–5 keV and 7–10 keV with a single power-law model ($\Gamma \sim -0.5$).

scattering (Yaqoob 1997). As expected, this model gives a column density of $\sim 1.1 \times 10^{24}$ cm^{-2}, slightly lower (though still consistent within the errors) than $\sim 1.3 \times 10^{24}$ cm^{-2} obtained with our baseline model. At equal column density, the model that includes Compton scattering is more effective (by ~ 20–30% between 6 and 30 keV) in reducing the transmitted spectrum. The fit with $plcabs$ is statistically slightly worse than the one obtained with our baseline model ($\Delta\chi^2 \simeq 6$). A slightly steeper ($\Gamma \simeq 1.83$) high-energy power-law is obtained which, however, does not significantly change the other best-fit parameters (including the line parameters). The main consequences of this correction are thus in the calculations of the source luminosity that strongly depends on the $N_{\rm H}$ and Γ values used. With the $plcabs$ model, the 0.1–150 keV luminosity is reduced to about 2.3×10^{44} ergs s^{-1}, compared to the value of 2.6×10^{44} ergs s^{-1} obtained with the baseline model.

Secondly, there are still residuals at energies between ~ 2 and 4 keV (Fig. 3), namely a broad absorption structure at ~ 3 keV and some excess emission at ~ 4 keV. Such excess counts indicate that the low-energy spectrum is probably more complex than a single power-law continuum, in agreement with *ASCA* results (Iwasawa 1995 (I95 hereinafter), G98). As suggested by these authors, thermal emission and/or absorption plus emission from a hot photo-ionized medium could be relevant in Mkn 3. Unfortunately, compared to the *ASCA* results, the poorer statistics of the LECS+MECS spectrum below ~ 4 keV does not allow a detailed modeling of these features. Alternatively, we note that such features could be due to fluorescence of elements lighter than iron expected from the reflection component (and not included in our model) as calculated by Reynolds et al. (1994). For example, the feature at ~ 4 keV could possibly be identified as a Calcium Kα fluorescence line emission (3.69 keV). In any case, the baseline best-fit parameters only weakly depend on the exact modeling of the soft component because variations by ~ 50% in the soft power-law slope af-

fect $N_{\rm H}$, $\Gamma_{\rm hard}$ and $A_{K\alpha}$ by less than 10%, i.e. less than the statistical errors reported in Table 1.

Thirdly, the power-law continuum of our baseline model represents only a phenomenological model. We thus tested a more physical and self-consistent model: the Comptonization model ($tita_a$ in XSPEC) calculated by Hua & Titarchuck (1995), that also includes reflection from optically thick gas. This model basically replaces the underlying power-law continuum with an exponential cutoff of our baseline model by a thermal Comptonization spectrum with reflection (Magdziarz & Zdziarski, 1995). The fundamental parameters of the model are the thermal gas optical depth (τ) and its temperature (kT). We find that the data can be reasonably well modeled ($\chi^2_{red} = 0.99$) by an intrinsic spectrum due to thermal Comptonization with $\tau \simeq 0.5 \pm 0.2$ and $kT \gtrsim 110$ keV (at the 90% confidence level for two interesting parameters).

Fourthly, the baseline model requires a broad iron line whose modeling is addressed in detail in the following section.

3.4. On the iron K line complex

It is interesting to note that if the shape of the continuum below the line (in the energy interval ~ 3–10 keV) is parameterized by a single power-law model (with $\Gamma = -0.5$), the line residuals (Fig. 5) suggest a complex profile. It comprises a red-shifted wing down to about 5 keV, a narrow and strong component peaking at ~ 6.4 keV plus a clear wing on the high-energy side of the line which drops at ~ 7 keV. A continuum $\Gamma = -0.5$ model is clearly unphysical and should rise doubts on the interpretation of the line profile obtained in this way. However, such multi-peaked structure may suggest a physical origin in an accretion disk (for the red and blue wings) plus a superposition of a narrow line at ~ 6.4 keV produced far from the black hole. Such conditions have been found in other Seyfert 2 galaxies often grouped under the name of Narrow Emission Line Galaxies (Weaver et al. 1997, Weaver & Reynolds 1998). However, contrary to what found by these authors in the sources they analyzed, in Sects. 3.1 and 3.2 we have shown that Mkn 3 certainly has a large absorption column which strongly affects the modeling of the underlying continuum between 3–10 keV. Indeed if we parameterize the continuum as given by our baseline model, we obtain the residuals shown in Fig. 6. Clearly, the red wing can be almost entirely explained by the combination of the reflection continuum and strong absorption. This illustrates the complexities of spectral modeling of emission lines when the underlying continuum is not well defined. The intrinsic power of broad band spectroscopy in sorting out these complexities and the advantage of using $BeppoSAX$ in this case are clearly evidenced.

However, Fig. 6 shows that "even" with our baseline model, the line appears complex with a significant excess emission at energies between 6.4–7 keV. Fitting the data with two narrow ($\sigma = 0$ eV) Gaussian lines yields a significantly better fit ($\Delta\chi^2 = 6$, for one more free parameter). The fit gives E$_1$ = $6.43^{+0.08}_{-0.08}$ keV, I$_1$ = $3.5^{+0.9}_{-1.0} \times 10^{-5}$ photons cm^{-2} s^{-1} (observed) for the neu-
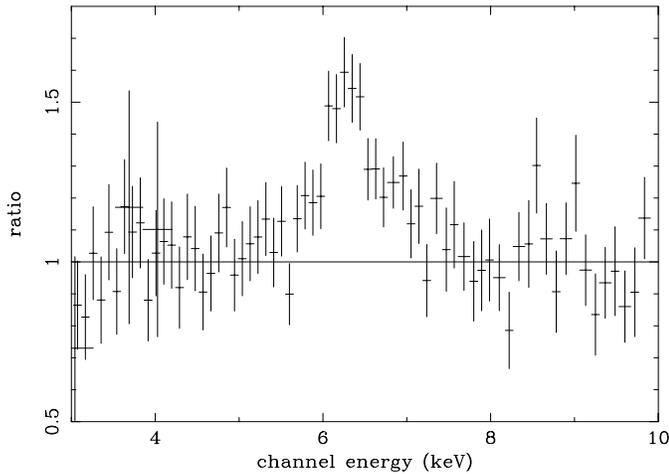
Fig. 6. Data to model ratios obtained from fitting the LECS + MECS + PDS spectrum between 0.8–5 keV and 7–100 keV with the baseline model (Table 1, line 4).

Fig. 7. Overplot of the *BeppoSAX* (MECS), *ASCA* (GIS) and *Ginga* (top-layer) unfolded spectra. See text for details. 3–10 keV data fitted with a single (inverted) power-law with Γ=-0.25.

tral fluorescence iron line and $E_2 = 7.00^{+0.23}_{-0.24}$ keV, $I_2 = 1.3^{+0.9}_{-0.9}$ $\times 10^{-5}$ photons cm^{-2} s^{-1} (observed) for the line at higher energies, respectively. These values are similar to the results previously found with *ASCA* (I94, G98, Netzer et al. 1998). The observed intensity of the neutral line corresponds to an equivalent width of $\simeq 645 \pm 180$ eV with respect to the reflection component and $\simeq 650 \pm 182$ eV with respect to the absorbed power-law continuum. The observed intensity of the line at higher energies corresponds to an equivalent width of $\simeq 235 \pm 160$ eV, $\simeq 164 \pm 113$ eV and $\simeq 6.2 \pm 4.3$ keV with respect to the reflection component, the absorbed power-law continuum and the (soft) scattered continuum, respectively.

From Fig. 6, there is also an indication of a weak red-wing of the 6.4 keV iron line that could be attributed to Compton down-scattering in optically thick, cold matter as found in the Seyfert 2 galaxy NGC 1068 by Iwasawa et al. (1997). Theoretical models predict that this Compton shoulder should contribute with an intensity about one tenth that of the line core (Matt et al. 1991). Unfortunately, we cannot reach any firm conclusion about this because the feature is not statistically significant in the data.

3.5. Long-term X-ray history of Mkn 3

The *observed* 2–10 keV flux (calculated with our baseline model) is 6.5×10^{-12} ergs cm^{-2} s^{-1} which places Mkn 3 in an intermediate state between its brighter state observed by *Ginga* in 1989 ($F_{2-10\,\text{keV}} \sim 6$–$10 \times 10^{-12}$ ergs cm^{-2} s^{-1}, depending on the adopted model: Awaki & Koyama 1993, I95, G98) and the fainter state measured by *ASCA* in 1993 ($F_{2-10\,\text{keV}} \sim 1.3$–$1.9 \times 10^{-12}$ ergs cm^{-2} s^{-1}, depending on the adopted model: I94, G98, Turner et al. 1997a).

Given the spectral complexity of Mkn 3, it is not straightforward to compare the present *BeppoSAX* results with previous X-ray observations because any residual feature (in particular the iron line intensity and continuum flux) is a strong function of the model adopted for the underlying continuum (see
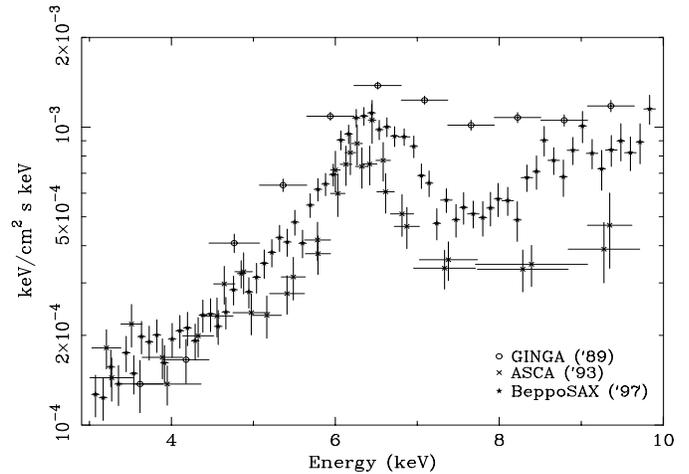
Appendix A) and also depends inevitably on the instrumental sensitivity and resolution. In order to provide a fair comparison, we thus re-analyzed the archival *ASCA* GIS and *Ginga* (upper-layer) data and compared it directly to the *BeppoSAX* MECS data. To reduce as much as possible the model-dependency in this comparison, we fitted each dataset only between 3–10 keV using a single power-law model with Γ fixed to -0.25 (the average value obtained from the 3 instruments) and free normalization. A direct comparison between the three unfolded spectra is shown in Fig. 7. Inspection of the figure reveals that i) the continuum above the line (E > 6.5 keV) decreased by about a factor of 4 between *Ginga* and *ASCA* and increased by about a factor 2 between *ASCA* and *BeppoSAX*, ii) the $\sim$ 5–6 keV continuum and Fe K$_\alpha$ line intensity varied significantly less, by a factor of about 2 between *Ginga* and *ASCA*, and by less than 50% between *ASCA* and *BeppoSAX* and iii) the 3–5 keV continuum did not vary at all. The slow responses of the Fe K$_\alpha$ line and 3–6 keV continuum to the flux variations clearly indicate that such variations cannot be due to pure transmission but need dilution by a constant component. The argument, in turn, is giving support to the results of our spectral analysis (Sect. 3.2) which require inclusion of a Compton reflection component. As a matter of fact, all observations are consistent with a variable direct component and associated (variable) transmitted Fe K$_\alpha$ line plus a constant reflection component and associated (constant) reprocessed Fe K$_\alpha$ line. The non-varying (reprocessed) Fe K$_\alpha$ line indicates that it did not respond to continuum variations occured 7 years apart and places a rough lower limit of $\sim$ 2 pc from the central source on the location of the Fe K$_\alpha$ line emitter. It should also be noted that the implication that the direct component of Mkn 3 varies with time is also supported by the observed increase (by a factor of $\sim$ 3) between the *OSSE* and *BeppoSAX* high energy fluxes (see Sect. 3.1).

In the soft (E< 3 keV) X-ray band, the *BeppoSAX* flux of $\sim 7.6 \times 10^{-13}$ ergs cm^{-2} s^{-1} between 0.6–3 keV (corresponding to a luminosity of $\sim 6 \times 10^{41}$ ergs s^{-1}) is comparable to

previous measurements with the *Einstein* IPC (Kruper et al. 1990), *BBXRT* (Marshall et al. 1992), *ROSAT* PSPC (Turner et al. 1993) and *ASCA* (I95). Therefore, as previously pointed out by I95, the lack of variability of the soft X-rays suggests that they originate from an extended region and immediately rules out a partial covering of the X-ray continuum which predicts that both hard and soft X-rays should vary simultaneously. Mkn 3 does not show evidence for starburst contamination (Pogge & De Robertis 1993) and Turner et al. (1997b) estimated a thermal emission in the 0.5–4.5 keV band lower than $\sim 6 \times 10^{40}$ ergs s^{-1} on the basis of its far infra-red luminosity. Therefore the most probable explanation for the lack of variations is that the soft X-rays are dominated by scattering of the intrinsic continuum (see also G98 and Netzer et al. 1998).

4. Discussion

The above results have shown that the broad-band spectrum of Mkn 3 is best described by the sum of a soft power-law, an *unabsorbed* reflection component, an iron line and a strongly absorbed hard power-law component. The most remarkable result of the present analysis is that the hard (E$\gtrsim$ 20 keV) X-ray spectrum is steep with $\Gamma \sim 1.8$ and that there is no evidence of a spectral break in the data for energies up to at least ~ 150 keV. The steep intrinsic spectrum is consistent with the canonical value found for Seyfert 1 galaxies (Nandra & Pounds 1994, Perola et al. 1999). The lack of a cutoff in our data is consistent with the large average value ($E_c \simeq 0.7^{+2.0}_{-0.3}$ MeV) found for a sample of 5 radio-quiet Seyfert 1 galaxies detected both by *OSSE* and *Ginga* (Gondek et al. 1996, Zdziarski et al. 1997). It is also consistent with the lower-limits ($E_c \gtrsim 150$ keV, Perola et al. 1999) and detections ($E_c \simeq 150$–200 keV, Piro et al. 1999) obtained with *BeppoSAX* for several Seyfert 1–1.5 galaxies. Both measurements thus support a unified model of Seyfert galaxies.

The very high absorption column density measured here makes Mkn 3 very similar to other known buried Seyfert 2 galaxies: NGC 4945 (Done et al. 1996), Circinus galaxy (Matt et al., in preparation) and possibly NGC 4941 (Salvati et al. 1997). As pointed out by Salvati et al. (1997), a better knowledge of the number of such heavily absorbed sources is extremely important because it has direct consequences on synthesis models of the X-ray background (Comastri et al. 1995, Gilli et al. 1999). In the 3–6 keV band, the spectrum of Mkn 3 requires a relevant contribution from reprocessed emission, namely an unabsorbed reflection component with associated iron emission line. The best-fit parameters obtained (R ~ 0.95, E(Fe K$_\alpha$) ~ 6.4 keV, and EW(Fe K$_\alpha$) ~ 650 eV with respect to the reflection component) are comparable to the theoretical values expected for a cold reflector covering a solid angle of $\sim 2\pi$ at the source (George & Fabian 1991, Matt et al. 1991). The long-term variability study suggests a distance of the reprocessor $\gtrsim 7$ light years (Sect. 3.5), that could thus be identified with an obscuring torus. Similar results have been found for example in NGC 2992 (Weaver et al. 1996), NGC 4151 (Piro et al. 1999) and NGC 4051 (Guainazzi et al. 1998). Moreover, a $\sim 2\pi$ covering

of the reprocessor is also consistent with a torus interpretation, provided that its half-opening angle is $\sim 45\%$.

In conclusion, both the strong absorption and unabsorbed reflection can be explained in the framework of unified models (i.e. assuming the existence of an optically thick torus). The absorption resulting from the transmission of the direct component through the rim of the torus. The reflection component (observed directly) resulting from reprocessing of the (same) direct component by the inner surface of the torus.

The origin of the second narrow line at higher energies is instead puzzling. Its energy (E ~ 7.0 keV) and intensity (EW $\sim 235 \pm 160$ eV) are roughly consistent with fluorescence iron Kβ emission from either the reflection component or the absorption component. Theoretical models would in fact predict (E ~ 7.06 keV and EW ~ 72 eV, assuming a Kβ/Kα ratio of 1:9, Matt et al. 1996). Alternatively, it could be interpreted as H- and/or He-like iron emission produced by the scattered soft component itself. Indeed, as shown by Matt et al. (1996), very strong resonantly scattered H- and He-like lines (with EW between 2–4 keV with respect to the scattered component, depending on the material optical depth and the line being strongest in the optically thin regime) are expected if warm material is responsible for the scattering. Given the large uncertainties in our measurement of its equivalent width, especially when calculated with respect to the soft scattered component (Sect. 3.4), such possibility cannot be excluded. There could also be a contribution from both Kβ fluorescence and resonant scattering. Moreover, we cannot exclude that both the weak red and blue wings of the Fe K$_\alpha$ line (Fig. 6) are produced by an additional reflection component (with associated diskline) from an accretion disk, as commonly observed in Seyfert 1 galaxies (Nandra & Pounds 1994, Perola et al. 1999) and, possibly, in some Narrow Emission Line Galaxies (Weaver & Reynolds 1998). Reflection from a highly inclined relativistic accretion disk would indeed produce extra emission at energies below and above the transmitted 6.4 keV Fe K$_\alpha$ line. In the case of Mkn 3, the effects of strong absorption and poor statistics hamper, however, a detailed modeling of such additional component that will require the use of more sensitive instruments like *AXAF* or *XMM*.

5. Summary

The main results derived from the present *BeppoSAX* observation of Mkn 3 are the following:

- Fit of the data above $\simeq 8$ keV require a strongly absorbed power-law, with $N_\mathrm{H} \simeq 1.3 \times 10^{24}$ cm^{-2}.
- The intrinsic high-energy power-law continuum is steep ($\Gamma \sim 1.8$) and shows no high-energy cutoff up to ~ 150 keV, similar to what is found in most Seyfert 1 galaxies.
- Having argued that a second absorbed power-law (i.e. a dual-absorber) is unlikely in this source, the data between ~ 2–10 keV require an unabsorbed reflection component to make the flat spectrum underlying the iron line.
- From the data fit and the long-term X-ray history of the source, the (neutral) iron line intensity is consistent with being produced in an obscuring torus placed at a distance
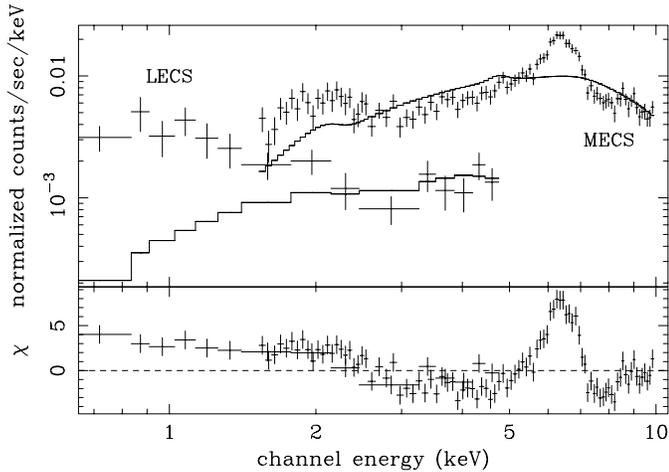
Fig. 8. LECS and MECS spectra and residuals with a continuum model consisting in a single power-law model ($\Gamma \sim -0.5$) absorbed by the Galactic absorption $N_{\mathrm{Hgal}} = 8.46 \times 10^{20} \mathrm{cm}^{-2}$.

of $\gtrsim 2\,\mathrm{pc}$ from the source partly by transmission through its rim and partly by reflection over its inner surface.

- Iron line emission is also detected at $\sim 7.0\,\mathrm{keV}$. It can be interpreted either as K_α emission associated to the neutral reflection component and/or to the absorption, either as H- and He-like Fe emission associated to the ionized soft scattered component, or a combination of the two. It could also be produced by an additional reflection component from a highly inclined relativistic accretion disk.

Overall, these results fit well into unified models scenarios of Seyfert galaxies and highlight the potentialities of using *BeppoSAX* in broad-band X-ray spectroscopy studies of buried sources like Seyfert 2 galaxies.

Appendix A: comparison with results and "ambiguities" from the literature for the data below 10 keV

To allow a direct comparison of the *BeppoSAX* results with the results reported in the literature (Sect. 1), we restrict here the analysis to the data below $10\,\mathrm{keV}$. In agreement with previous findings (G98 and ref. therein), the spectrum of Mkn 3 below $10\,\mathrm{keV}$ is very complex, with prominent soft excess emission below $3\,\mathrm{keV}$ and strong iron line emission above a flat underlying 3–$10\,\mathrm{keV}$ continuum. This is clearly illustrated by the residuals shown in Fig. 8 obtained by simultaneously fitting the LECS and MECS data with a single power-law model, with an extremely flat best-fit photon index $\Gamma \sim -0.5$.

The three basic descriptions for the continuum shown here (Table A1) comprise **a)** a double power-law model; **b)** a soft
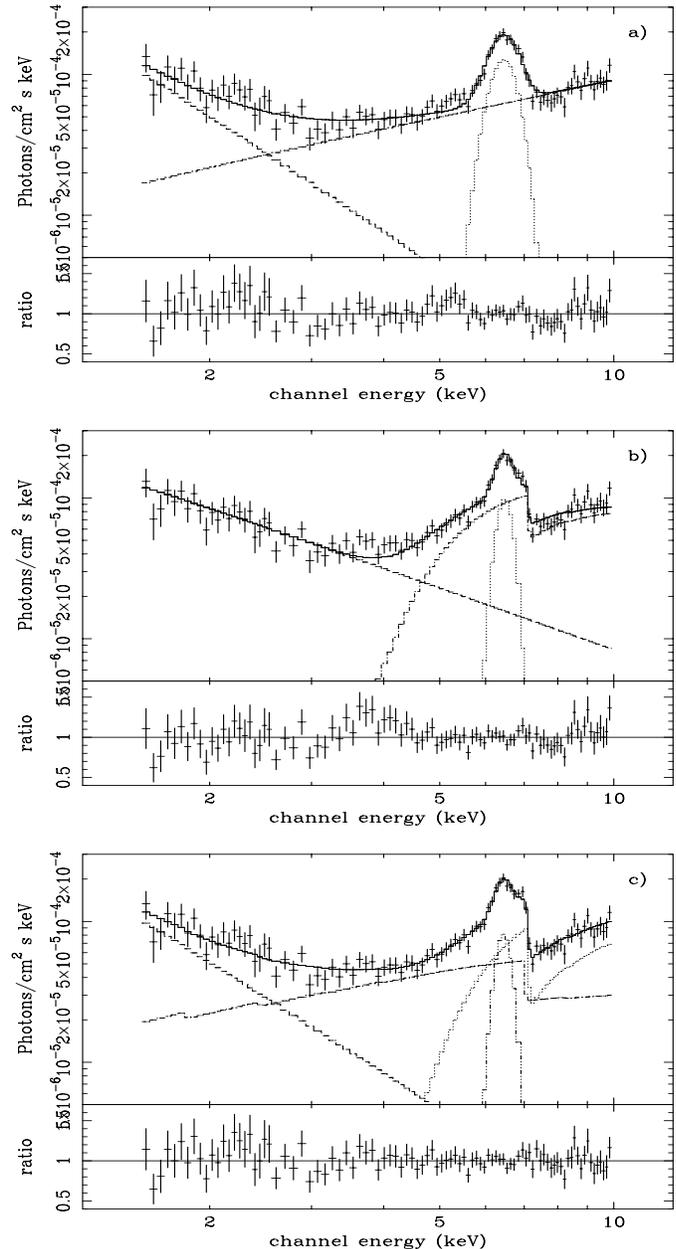

Fig. 9a–c. Unfolded spectra with best-fit models as obtained from the fits of the LECS+MECS data. Pannels **a**, **b** and **c** correspond to lines 1, 2 and 3 of Table A1, respectively. For clarity, only the MECS data have been plotted here.

power-law plus a hard, absorbed, power-law model; and **c)** model b) plus an *unabsorbed* pure reflection continuum model. A Gaussian emission line is added in all fits. The resulting best-fit parameters are given in Table A1.

We find that model c gives the best description of the data at energies lower than $10\,\mathrm{keV}$, with a $\Delta\chi^2 \sim 35$ compared with model b for one additional free parameter, in agreement with Turner et al. (1997b). However, it is difficult to clearly prefer one model to the other. Inclusion in model b of extra emission/absorption features in the soft and/or hard component (rather plausible if the scattering gas and/or absorbing material

Table A1. "Literature" models fitted to the data below 10 keV (LECS + MECS data)

Continuum Models[a]	Γ_s	A_s/A_h[b]	N_H[c]	Γ_{hard}	R	E_{K_α}[d]	σ_{K_α}[e]	A_{K_α}[f]	χ^2_{red}/χ^2/d.o.f.
model a: $pl_s + pl_h$	$2.78^{+0.53}_{-0.58}$	29.1	-	$-0.86^{+0.11}_{-0.11}$	-	$6.54^{+0.05}_{-0.04}$	$0.37^{+0.05}_{-0.06}$	$11.7^{+1.3}_{-1.2}$	1.10/116/105
model b: $pl_s + abs.\ pl_h$	$1.28^{+0.09}_{-0.09}$	0.072	65^{+4}_{-6}	$\equiv\Gamma_{soft}$	-	$6.52^{+0.13}_{-0.03}$	$0.21^{+0.12}_{-0.07}$	$5.8^{+1.2}_{-1.0}$	1.21/127/105
model c: $pl_s + refl. + abs.\ pl_h$	$2.68^{+0.41}_{-0.50}$	0.021	125^{+23}_{-17}	$1.79^{+0.2}_{-0.18}$	$0.95^{+0.5}_{-0.2}$	$6.48^{+0.14}_{-0.04}$	$0.22^{+0.16}_{-0.20}$	$4.4^{+1.3}_{-1.5}$	0.88/92/104

[a] See text for a description of the models and parameters used; [b] Ratio of the power-law normalizations calculated at 1 keV; [c] In units of $10^{22}\ cm^{-2}$. [d] Line energy in the source rest-frame, in units of keV; [e] Line width, in units of keV; [f] *Observed* line intensity in units of 10^{-5} photons $cm^{-2}\ s^{-1}$.

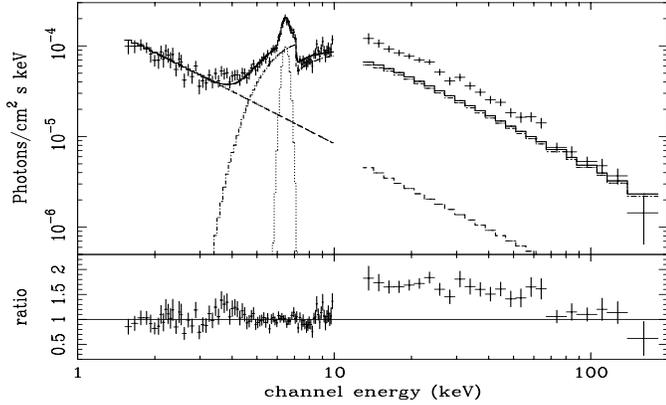*Note:* Intervals are at 90% confidence for 2 interesting parameters.

Fig. 10. Unfolded spectrum with the best-fit model b) as obtained from the fit of the LECS+MECS data and with the PDS data added subsequently.

is ionized) could account for most of the remaining residuals of the fit (i.e, the 3–5 keV bump, iron edge structure and excess emission above ~ 7 keV, as shown in Fig. 9b). This ambiguity is similar to the one resulted from the *ASCA* data that led to different parameterizations and interpretation of the same data by different authors (I94, Turner et al. 1997b, G98). However, we have shown in Sect. 3.2 how such an ambiguity can be solved thanks primarily to the *BeppoSAX* detection of the high-energy ($E \gtrsim 10$ keV) emission. This is also illustrated in Fig. 10 which shows that an extrapolation of model b) to higher energies falls short of the PDS data, thus requiring a more complex model with larger absorption.

Because of the spectral complexity, we also find that any residual feature is a strong function of the adopted model for the underlying continuum. For example, from the ratios shown in Figs. 9a, 9b and 9c there is some evidence of a broad absorption structure between ~ 7–8 keV that, at first glance, could be ascribed to absorption by ionized material (G98). However, a comparison of the different figures shows that the feature is significant within model a and model b but is only marginal in model c. Indeed, in our baseline model, such an edge is entirely accounted for ($\tau \lesssim 0.5$ if an extra absorption edge is added at energies between 7–8 keV) by the combination of the deep Fe

K edge of the large absorption column density plus the broad Fe K edge produced by the reflection component.

Moreover, as shown in Table A1, the same data give differences of about a factor of two in the line width (and thus line intensity) depending on the adopted continuum model. Even for equal width (compare lines in pannels b and c of Fig. 9), a different continuum modeling can result in a $\sim 20\%$ difference in the *observed* line intensity.

In conclusion, the above results highlight the need of broad-band spectroscopy for such complex sources in order to reach confidence that the continuum emission and spectral features are properly modeled.

Appendix B: alternative models to our baseline model

More complex models have also been fitted to the *BeppoSAX* broad-band spectrum, in particular: a *neutral* dual absorber model and a dual absorber model with a mixture of neutral and ionized matter. The basic idea is to explain the flat ~ 3–10 keV underlying continuum without using an *unabsorbed* reflection component (as proposed in our baseline model, Sect. 3.2) but with the addition of a second absorbed power-law component. The former model has been extensively used in the literature to explain complex absorption and/or flat 2–10 keV spectra of several Seyfert galaxies (EXO 055620–3820.2, Turner et al. 1996; NGC 4151, Weaver et al. 1994; NGC 5252, Cappi et al. 1996; NGC 2110, Hayashi et al. 1996, Malaguti et al., 1999; NGC 7172, Guainazzi et al. 1997; IRAS 04575-7537, Vignali et al. 1998). The latter model has been first proposed by G98 for Mkn 3 based primarily on the *Ginga* detection of an ionized Fe K edge at $E \sim 8$ keV. The results obtained with these models are given in Table B1. The ionized absorber model used here is the *absori* model in XSPEC (Done et al. 1992) with a temperature fixed to 10^6 K, as in G98 (none of the following conclusions changed, though, for a temperature ranging between 10^{4-6} K). We find that both models give acceptable fits of the broad band spectrum and are both statistically indistinguishable given our data alone. None of them, however, gives a statistically better fit than the baseline model (Sect. 3.2, Table 1) considering the increase by 1 and 2 in the number of free parameters for the former and latter model, respectively. Given the poor statistics of the data at low energies, we did not attempt to fit a more physical (and

Table B1. Alternative models fitted to the broad band spectrum (LECS + MECS + PDS data)

Continuum Model[a]	Γ_s	$A_s/A_h(1)$ $\times 10^{-2}$	$N_H(1)$[b]	$\Gamma_h(1)$ $\equiv \Gamma_h(2)$	$N_H(2)$[b]	C_f^c	ξ	E_{K_α}[d]	σ_{K_α}[e]	A_{K_α}[f]	χ^2_{red}/χ^2/d.o.f.
$pl_s+abs(2)pl_h(2)+abs(1)pl_h(1)$	$1.89^{+0.51}_{-0.44}$	1.9	133^{+50}_{-24}	$1.75^{+0.13}_{-0.12}$	23^{+13}_{-9}	$0.92^{+0.04}_{-0.02}$	-	$6.46^{+0.10}_{-0.02}$	$0.25^{+0.12}_{-0.12}$	$5.5^{+1.6}_{-1.3}$	$0.91/\ 118/130$
$pl_s+warm(2)pl_h(2)+abs(1)pl_h(1)$	$2.10^{+0.58}_{-0.55}$	2.0	127^{+34}_{-15}	$1.75^{+0.09}_{-0.08}$	52^{+28}_{-32}	$0.93^{+0.03}_{-0.03}$	66^{+64}_{-58}	$6.46^{+0.07}_{-0.08}$	$0.20^{+0.12}_{-0.15}$	$4.9^{+4.8}_{-1.8}$	$0.89/115/129$

[a] See text for descriptions;
[b] In units of 10^{22} cm^{-2};
[c] Covering factor, equivalent to $A_h(1)/(A_h(1)+A_h(2))$;
[d] Line energy in the source rest-frame, in units of keV;
[e] Line width, in units of keV;
[f] *Observed* line intensity in units of 10^{-5} photons cm^{-2} s^{-1}.

more complex) model for the ionized absorber that would take into account emission/reflection from the absorbing gas or the possible presence of dust.

Moreover, the main problem with both these models is that, in order to interpret physically different absorbing columns along our line of sight, one is forced to assume either that i) the source of X-rays is not a point source as seen from the two absorbers *and* the two different columns cover different areas of the source or that ii) the lowest of the two column densities covers the whole source while the larger one only partially covers it. The former geometry appears rather unlikely given the small dimensions generally inferred to the X-ray emitting regions in AGNs from variability arguments (e.g. Mushotzky et al. 1993). The latter geometry could be more physical and fits well into the framework of Unified Models since one could identify the highest column density ($N_H(1)$ in Table B1) with the BLR clouds, partially covering the source, and the lowest column ($N_H(2)$) with absorbing matter, eventually ionized, associated with the torus (or its rim) or with some matter in the outer zone of the galaxy (e.g. Hayashi et al. 1996, Vignali et al. 1998). However, our best-fit results give $N_H(1) \sim 1.2 \times 10^{24}$ cm^{-2} and a covering fraction of 90% (Table B1, column 7) which are at least an order of magnitude larger than commonly believed for the BLR (respectively 10^{22-23} cm^{-2} and 5–30%, Netzer & Laor 1993, Kwan & Krolik 1981). Such complex models may, possibly, also find alternative interpretations in terms of different geometries involving complex scattering by matter at non-uniform density and/or with non-uniform coverage.

It should also be noted that the main reason G98 proposed an ionized absorption model was the presence of an ionized Fe K absorption edge in the *Ginga* data at ~ 7–8 keV. However our MECS 7–10 keV data, with unprecedent statistics, show that such edge could be entirely accounted for by the combination of the reflection component and the larger column density (required by the PDS data) as given in our baseline model (Sect. 3.2). In conclusion, we find no need from the present data to invoke more complex models and/or to invoke ionized absorption in our data.

References

Antonucci R.R.J., 1993, ARA&A 31, 473

Arnaud K.A., 1996, In: Jacoby G., Barnes J. (eds.) Astronomical Data Analysis Software and Systems V, ASP Conf. Series volume 101, p. 17

Awaki H., Koyama K., 1993, Adv. Space Res. vol. 13, 12, 221

Awaki H., Koyama K., Inoue H., Halpern J.P., 1991, PASJ 43, 195

Bassani L., Malaguti G., Jourdain E., Roques J.P., Johnson W.N., 1995, ApJ 444, L73

Bassani L., Dadina M., Maiolino R., et al., 1998, ApJS in press

Boella G., Chiapetti L., Conti G., et al., 1997, A&AS 122, 327

Cappi M., Mihara T., Matsuoka, et al., 1996, ApJ 456, 141

Chiappetti L., Dal Fiume D., 1997, In: Scarsi L., Maccarone M.C. (eds.) Proceedings of 5th International Workshop on Data Analysis in Astronomy

Comastri A., Setti G., Zamorani G., Hasinger G., 1995, A&A 296, 1

Cusumano G., Mineo T., Guainazzi M., et al., 1998, A&A in press

Dickey J.M., Lockman F.J., 1990, ARA&A 28, 215

Done C., Madejski G.M., Smith D.A., 1996, ApJ 463, L63

Done C., Mulchaey J.S., Mushotzky R.F., Arnaud K.A., 1992, ApJ 395, 275

Frontera F., Costa E., Dal Fiume D., et al., 1997, In: Proceedings of EUV, X-ray, and Gamma-ray Instrumentation for Astronomy VIII, SPIE, 3114, 206

George I.M., Fabian A.C., 1991, MNRAS 249, 352

Ghisellini G., Haardt F., Matt G., 1994, MNRAS 267, 743

Gilli R., Comastri A., Brunetti G., Setti G., 1999, New Astronomy, in press

Gondek D., Zdziarski A.A., Johnson W.N., et al., 1996, MNRAS 282, 646

Grandi P., Haardt F., Ghisellini, et al., 1998, ApJ 498, 220

Griffiths R.G., Warwick R.S., Georgantopoulos I., Done C., Smith D.A., 1998, MNRAS 298, 1159

Guainazzi M., Matt G., Antonelli A., et al., 1997, MNRAS 298, 824

Guainazzi M., Nicastro F., Fiore F., et al., 1998, MNRAS 301, L1

Haardt F., 1997, Mem. Soc. Astron. Ital. 68, 73

Haardt F., Fossati G., Grandi P., et al., 1998, A&A 340, 35

Haniff C.A., Wilson A.S., Ward M.J., 1988, ApJ 334, 104

Hayashi I., Koyama K., Awaki H., Ueno S., Yamauchi S., 1996, PASJ 48, 219

Hua X.-M., Titarchuck L., 1995, ApJ 449, 188

Iwasawa K., 1995, Ph.D. Thesis (I95)

Iwasawa K., Yaqoob T., Awaki H., Ogasaka Y., 1994, PASJ 46L, 167, (I94)

Iwasawa K., Fabian A.C., Matt G., 1997, MNRAS 289, 443

Kruper J.S., Canizares C.R., Urry C.M., 1990, ApJS 74, 347

Kwan J., Krolik J.H., 1981, ApJ 250, 478

Magdziarz P., Zdziarski A.A., 1995, MNRAS 273, 837

Maisack M., Johnson W.N., Kinzer R.L., et al., 1993, ApJ 407, L61

Malaguti G., Bassani L., Cappi M., et al., 1999, A&A 342, L41

Manzo G., Giarrusso S., Santangelo A., et al., 1997, A&AS 122, 341

Marshall F.E., Boldt E.A., Holt S.S., et al., 1992, In: Tanaka Y., Koyama K.(eds.) Frontiers of X-ray Astronomy. Proc. of the 28th Yamada Conference, Nagoya, Japan, Universal Academy Press, p. 233

Matt G., Perola G.C., Piro L., 1991, A&A 247, 25

Matt G., Brandt W.N., Fabian A.C., 1996, MNRAS 280, 823

Miller J.S., Goodrich R.W., 1990, ApJ 355, 456

Mushotzky R.F., Done C., Pounds K.A., 1993, ARA&A 31, 717

Nandra K., Pounds K.A., 1994, MNRAS 268, 405

Netzer H., Laor A., 1993, ApJL 404, 51

Netzer H., Turner T.J., George I.M., 1998, ApJ 504, 680

Parmar A.N., Martin D.D.E., Bavdaz M., et al., 1997, A&AS 122, 309

Perola G.C., et al., 1999, to appear in: Proceedings of Dal nano- al tera-eV: tutti i colori degli AGN. Third Italian conference on AGNs, Roma, Memorie S.A.It

Piro L., et al., 1999, to appear in: Adv. in Space Research, proceedings of The 32nd COSPAR Meeting, Broad Band X-ray Spectra of Cosmic Sources.

Pogge R.W., De Robertis M.M., 1993, ApJ 404, 563

Reynolds C.S., Fabian A.C., Makishima K., Fukazawa Y., Tamura T., 1994, MNRAS 268, L55

Salvati M., Bassani L., Della Ceca, et al. 1997, A&A 323, L1

Svensson R., 1994, ApJS 92, 585

Tran H.D., 1995, ApJ 404, 565

Turner T.J., Netzer H., George I.M., 1996, ApJ 463, 134

Turner T.J., Urry C.M., Mushotzky R.F., 1993, ApJ 418, 653

Turner T.J., George I.M., Nandra K., Mushotzky R.F., 1997a, ApJS 113, 23

Turner T.J., George I.M., Nandra K., Mushotzky R.F., 1997b, ApJ 488, 164

Vignali C., Comastri A., Stirpe G.M., et al., 1998, A&A 333, 411

Weaver K.A., Reynolds C.S., 1998, ApJ 503, L39

Weaver K.A., Yaqoob T., Holt S.S., et al., 1994, ApJ 436, L27

Weaver K.A., Nousek J., Yaqoob T., et al., 1996, ApJ 458, 160

Weaver K.A., Yaqoob T., Mushotzky R.F., et al., 1997, ApJ 474, 675

Weaver K.A., Krolik J.H., Pier E.A., 1998, ApJ 498, 213

Wilson A.S., Ward M.J., Haniff C.A., 1988, ApJ 334, 121

Yaqoob T., 1997, ApJ 479, 184

Zdziarski A., Johnson W.N., Done C., Smith D., McNaron-Brown K., 1995, ApJ 438, L63

Zdziarski A., Johnson W.N., Poutanen J., Magdziarz J., Gierlinski M., 1997, In: Courvoisier T.J.-L., Durouchoux Ph., Winkler C. (eds.) Proceedings of the 2nd Integral Workshop: The Transparent Universe. ESA SP-382, 373